

# POLITECNICO DI TORINO

Corso di Laurea Magistrale  
in Ingegneria Biomedica

Tesi di Laurea Magistrale

## Dose Management and Visualization



*Author:*  
Gianmarco Brusca

*Supervisor:*  
Prof. Filippo Molinari  
Prof. Wolfgang Recheis  
Prof. Michael Verius

Anno Accademico 2020/2021



POLITECNICO DI TORINO

## *Abstract*

Biomedical Engineering

### **Dose Management and Visualization**

by Gianmarco Brusca

The introduction of new interventional procedures led to introduce new regulations concerning patient safety from radiation dose. To cope with recent regulations, automatic software was born for dose management and visualization. This software get dose and geometry information of procedures through DICOM RDSR, generated by radiological equipment. After that, the software elaborates data, introducing the correction factors and geometry relation, obtaining a 3D visualization of the patient with color code indication for irradiated areas of the body. The correction factors used for this project, allow to conversion of the Reference Air Kerma to skin absorbed dose. The final result, peak skin dose, is necessary to assess possible skin injuries and inform the interested clinician. In particular, this project has been developed in University Hospital of Innsbruck, allowing to use the patient database and the following devices: Philips FD 20, Siemens Axiom Artis Zee and Siemens Fluorospot S1. The software has been executed in Ubuntu 18.04 LTS with GNU GCC compiler, dcmtk library and Apache Web Server.



## *Acknowledgements*

I would like to sincerely thank all the people who were helpful to reach this important milestone. In particular, thank you:

Prof. Filippo Molinari, Prof. Wolfgang Recheis, Prof. Michael Verius and Prof. Robert Eder for giving me possibility to carry out this amazing project.

My family, friends and girlfriend for supporting me financially and emotionally during this long period.



# Contents

<b>Abstract</b>	<b>iii</b>
<b>Acknowledgements</b>	<b>v</b>
<b>1 Introduction</b>	<b>1</b>
<b>2 Purpose</b>	<b>5</b>
<b>3 State of Art</b>	<b>7</b>
<b>4 Fluoroscope components description</b>	<b>11</b>
4.1 C-arm . . . . .	11
4.2 X-ray tube . . . . .	11
4.3 Detector . . . . .	12
4.4 Operating console . . . . .	13
<b>5 Digital Imaging and Communications in Medicine (DICOM)</b>	<b>15</b>
5.1 Radiation Dose Structured Report (RDSR) . . . . .	16
<b>6 Phantom</b>	<b>19</b>
<b>7 Geometry</b>	<b>23</b>
<b>8 Parameters</b>	<b>27</b>
<b>9 Absorbed dose calculation</b>	<b>29</b>
9.1 Reference Air Kerma . . . . .	29
9.2 Correction source to skin distance . . . . .	30
9.3 Backscatter factor . . . . .	31
9.4 Correction from air kerma to skin kerma . . . . .	32
9.5 Correction for patient support table . . . . .	34
9.6 Summary of correction factor . . . . .	34
<b>10 Environment setup</b>	<b>37</b>
<b>11 Software information and architecture</b>	<b>39</b>
<b>12 Libraries description</b>	<b>43</b>
12.1 RDSRparse.h . . . . .	43
12.2 PatientBeamAlignmentGeometry.h . . . . .	44
12.3 SurfaceXRay.h . . . . .	45
12.4 DSRreports.h . . . . .	45
12.5 HTML.h . . . . .	46
<b>13 Visualization</b>	<b>49</b>

<b>14 Test and results</b>	<b>53</b>
<b>15 Future work</b>	<b>59</b>
<b>A Parameter description</b>	<b>61</b>
<b>Bibliography</b>	<b>65</b>

# List of Figures

3.1	Examples of SDM software outputs (Malchair et al., 2020).	9
4.1	X-ray tube.	12
4.2	Biplane Philips FD 20.	13
4.3	Biplane Siemens Axiom Artis Zee.	14
4.4	Siemens Fluorospot Compact S1.	14
5.1	Example of VM from DICOM standard.	16
5.2	Example of "tag" from DICOM standard.	16
5.3	Hierarchical structure of RDSR.	17
6.1	Phantom models for Skin Dose Map.	21
6.2	Frontal view of scaled adult female armless phantom.	22
7.1	Phantom reference system.	23
7.2	Operating table reference system.	23
7.3	C-arm reference system.	24
7.4	Isocenter reference system.	24
7.5	Patient position approaches.	25
9.1	Transverse view of IR equipment.	31
9.2	Interpolation of MC simulated data for BSF.	32
9.3	Interpolation of MC simulated data for $k_{med}$ .	33
9.4	Experiment for the extrapolation of $k_{(T+P)}$ (Hellström, 2018).	35
11.1	Flowchart of Skin Dose Map calculation.	39
12.1	Example of GET functions in RDSRparse.h.	44
12.2	System coordinates representation.	44
12.3	Example of RDSR x-ray event.	45
13.1	Web page Skin Dose Map.	49
13.2	(a) Left column of SDM. (b) Right column of SDM.	51
13.3	(a) View of lateral plane. (b) View of frontal plane. (c) View of transverse plane.	51
14.1	TLDs placement from slice 12th to 19th of phantom.	53
14.2	Setup for test.	54
14.3	(a) Radiography of head and RaySafe Xi detector. (b) Chest radiography of phantom. (c) Skin dose map.	55
14.4	Example of software output in <i>output.txt</i> .	55
14.5	(a) TLDs test. (b) Setup for TLDs test.	55
14.6	Dose distribution along x axis per slice.	57
14.7	Mean values of absorbed dose per slice.	58

A.1 Positioner Primary Angle. . . . .	61
A.2 Positioner Secondary Angle. . . . .	61

# List of Tables

1.1	Radiation quantities . . . . .	2
1.2	Skin injuries (Wunderle, 2016) . . . . .	3
3.1	List of available Skin Dose software . . . . .	8
6.1	PCXMC phantom dimension. . . . .	20
8.1	List of general parameters . . . . .	27
8.2	List of specific parameters per event . . . . .	28
14.1	Results of TLDs test . . . . .	56
14.2	Values of histograms . . . . .	58
A.1	Description of RDSR parameters . . . . .	62



# List of Abbreviations

<b>2D</b>	Two - Dimensional
<b>3D</b>	Three - Dimensional
<b>SDM</b>	Skin Dose Map
<b>ICRP</b>	International Commission on Radiological Protection
<b>DICOM</b>	Digital Imaging and Communications in Medicine
<b>RDSR</b>	Radiation Dose Structured Report
<b>IOD</b>	Information Object Definition
<b>CID</b>	Context Group ID
<b>VR</b>	Value Representation
<b>VM</b>	Value Multiplicity
<b>BREP</b>	Boundary REpresentation Phantom
<b>HC</b>	Head Centric Approach
<b>TC</b>	Target Centric Approach
<b>SID</b>	Source to Isocenter Distance
<b>SDD</b>	Source to Detector Distance
<b>IRP</b>	Interventional Reference Point
<b>BSC</b>	BackSCatter Factor
<b>HVL</b>	Half Value Layer
<b>FSL</b>	Field Side Length



## Chapter 1

# Introduction

In the last few decades, the introduction of more sophisticated devices in interventional radiology led to an improvement in the procedures and, at the same time, an increase in the x-ray exposure of patients. These devices allow to inspect several parts of the body in non-invasive procedures, usually on the heart, head, liver, blood vessels. The patient lies down on a movable table and the operator places the x-ray unit in the right site of the body using a console from which manages even the acquisition type. With the pulsed x-ray imaging it is possible to navigate with a low quality image (Fluoroscopy) searching the right diagnostic spot or following the lead in the blood vessels, for example, during a pacemaker placement, and once on site can be obtained a high quality image injecting a contrast medium (Stationary Acquisition). At every acquired image, fluoroscopy or stationary acquisition, correspond to a certain amount of dose that can be different from each other, normally, the fluoroscopy requires a low dose but if used for a long time can reach the dose of the stationary acquisition. Depending on the number of acquired images, the patient is subjected to several x-ray exposures which can cause different skin injuries. The x-rays are classified as ionizing radiation which has a biological effect on the anatomical structures they pass through. Ionizing radiation damages the cellular DNA and leads to cellular death. The damages can be divided into deterministic somatic, where effects depend on overcoming a threshold above which tissue reactions increase in gravity proportional to the increment of dose, and in stochastic somatic, based on the statistical likelihood causing an effect.

When it comes to radiation, the International Commission on Radiological Protection (ICRP) defines the main radiation quantities to quantify the radiation dose

TABLE 1.1: Radiation quantities

Radiation quantity	SI, traditional unit	Definition
Exposure (X)	Coulomb/kg (C/kg), roentgen (R)	The amount of charge liberated per unit mass of air
Absorbed dose (D)	Gray (Gy), radiation absorbed dose (rad)	The amount of energy absorbed per unit mass of the absorbing medium
Air kerma	Gray (Gy)	The kinetic energy released in air; at photon energies used for diagnostic imaging, this quantity is very close to the absorbed dose in air
Air kerma at the interventional reference plane ( $K_{a,r}$ )	Gray (Gy)	The air kerma determined at the interventional reference plane, defined as 15 cm toward the X-ray tube from the isocenter of the fluoroscope c-arm gantry. This is the quantity displayed on most modern fluoroscopes
Peak skin dose ( $D_{skin,max}$ )	Gray (Gy)	The highest absorbed dose to the skin

absorbed by biological tissue (Table 1.1) (ICRP, 2007). Concerning this project, the quantities for evaluating the absorbed dose in the patient skin is  $D_{skin,max}$  but is unusual to find it in the last generation devices, so is used the standard value  $K_{a,r}$ , present in all new radiological systems, obtained by an ionization changer mounted on top of the x-ray collimator.

The ICRP classifies the radiation injuries compared to the amount of absorbed dose to the skin as shown in the Table 1.2 (Valentin, 2007).

The irradiation doses and latency do not correspond to fixed thresholds, but the effects can vary by individual for different reasons: previous illnesses, patient-specific factors such as smoking, obesity, the presence of overlapping skin folds, poor nutrition, and pre-existing skin degradation in the irradiated area; genetic disorders such as ataxia telangiectasia, Gorlin syndrome, Fanconi anemia, Bloom syndrome, xeroderma pigmentosum, familial polyposis, Gardner syndrome, hereditary malignant melanoma, and dysplastic nevus syndrome; diseases such as scleroderma, systemic lupus erythematosus, rheumatoid arthritis, hyperthyroidism, and diabetes mellitus; and the concurrent use of certain drugs such as doxorubicin, tamoxifen, methotrexate, bleomycin, 5-fluorouracil, and actinomycin D (Hymes, Strom, and Fife, 2006; Herold, Hanlon, and Hanks, 1999; Koenig et al., 2001). In order to prevent

TABLE 1.2: Skin injuries (Wunderle, 2016)

SINGLE IRRADIATION PEAK SKIN DOSE	APPROXIMATE REACTION LATENCY			
	Prompt (hours to 2 weeks)	Early (2-8 weeks)	Mid (6-40 weeks)	Late (>40 weeks)
<2 Gy	No effect predicted			
2-5 Gy	Mild pruritus, transient erythema		No effect predicted	
5-10 Gy	Intense pruritus, transient erythema	Dyspigmentation, edema, epilation, erythema		Dermal atrophy, telangiectasia
10-15 Gy		Dyspigmentation, desquamation (wet or dry), edema, epilation, erythema, necrosis, ulceration		
>15 Gy	Desquamation (wet or dry), edema, pruritus, transient erythema			Dermal atrophy, necrosis, telangiectasia, ulceration

these injuries, the device manufacturers in the first place included a monitor which is showed the amount of dose delivered by the machine during the examination, so the operator can be warned in case of high exposure and in the new ones is even possible to find an estimation of the peak skin dose.

Concurrently, the DICOM standard has been updated in the years defining the criteria for communication, archiving and visualization of the data generated from medical devices. From 1996, the Radiation Dose Structured Report has been introduced in the standard, which contains the dose and geometry information concerning the examination, allowing third parties to consult this report for the improvement of dose management.



## Chapter 2

# Purpose

In case of patients that need several examinations in a short period, the only way to prevent skin injuries, due to summation of dose for multiple examinations in the same region, is the monitoring of the previous ones. For the protection of the patient is necessary to implement a study of its antecedent data stored in order to know the maximum dose absorbed and its distribution in the patient skin, so that the operator can plan to perform the new examination differently, for example with different angulation, trying to limit the occurrence of tissue damage. In the last few decades were born software for dose management allowing to extract the needed information from the RDSR and later estimate the distribution of the radiation dose in the patient skin. Thanks to the digital archive of the hospital structure, is possible to acquire the entire radiological story of patients and generate an automatic software for dose management, taking care of the threshold for acute skin effects.



## Chapter 3

# State of Art

According to Data Bridge Market Research, it has been estimated the amount of global radiation dose management market to USD 227.59 million in 2018 growing at a CAGR (Compounded Average Growth Rate) of 41.1% during the forecast period 2019 to 2026.

Today, on the international market can be found a total of 22 products developed after 2000 in research-based institutions or for commercial purposes (Table 3.1) (Malchair et al., 2020). The main feature that distinguishes the products is the capability to work online during the examination using the live data streaming from the angiographic system and only 4 companies work in this manner. The alternative solution is the data stored in the RDSR, generated only after the examination. They differ even for the illustration choice of the results: from simple illustration of values to more sophisticated solutions calculating a 2D or 3D distribution of the skin dose (Figure 3.1).

Only 12 software validated with phantom measurements present an acceptable accuracy within 25%, cause the different implementation of specific correction factors to convert the Reference Air Kerma in Skin Dose. All products are machine-dependent, they have been tested for no more than two devices of different manufacturer because every system generates a different RDSR and present different reference for measurements.

TABLE 3.1: List of available Skin Dose software

<b>Software Name</b>	<b>Company name</b>
Dose Map	GE healthcare
Dosewatch	GE healthcare
DTS	CANON Medical Systems
em.dose	ESPRIMED
Radimetrics	BAYER
RDM	MEDSQUARE
DOSE	QAEUM
UF-RIPSA	Non-commercial
MCAR	Non-commercial
FDEIR	Non-commercial
MCGPU	Non-commercial
TeamPlay	SIEMENS Healthineers
Dosewise	PHILIPS
Dosetrack	SECTRA
Nexodose	BRACCO
Dose monitor	PACSHEALTH
Dosem	INFINITT
OpenSkin	Open Source
PySkinDose	Open Source
SkinCare	Open Source
CAATSDOSE	CAATS
DIDO	Hospital San Carlos Madrid Madrid

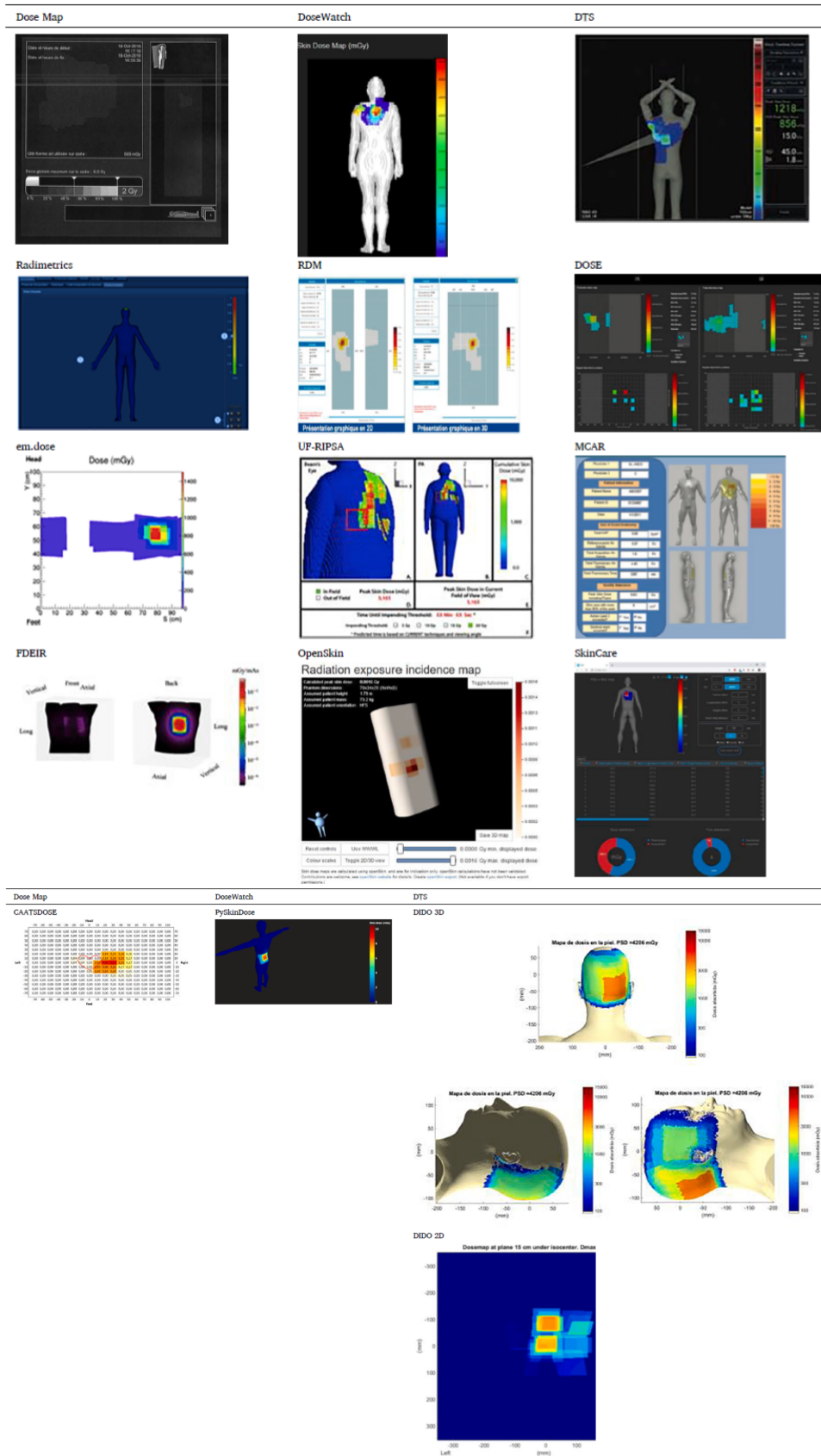


FIGURE 3.1: Examples of SDM software outputs (Malchair et al., 2020).



## Chapter 4

# Fluoroscope components description

A fluoroscope is an x-ray generator that provides real-time radiographic imaging. Fluoroscopic equipment is an interventional imaging device generally composed of C-arm, x-ray tube, detector, operating console and commonly this equipment is accompanied by a large monitor to see in real-time the current image and correlated parameters.

### 4.1 C-arm

A C-arm is a robotic semi-circular arm wherein the ends are affixed the x-ray tube, typically below the table, and on the opposite side the detector. The C-arm support system can be placed on the floor or mounted in a rail system fixed on the ceiling. In modern devices, the C-arm may be translated along with the table and rotated to the rotational centre for 360 degrees.

### 4.2 X-ray tube

The x-ray tube consists of an evacuated glass or metal enclosed assembly, a cathode that generates charges or rather energy and an anode used as the target. The cathode is a tungsten filament that is heated for current flowing emits electrons and increasing the velocity by a potential difference is obtained the anode shelling in a small area, known as focal spot track, and subsequently the x-ray production. The main

problem is the management of heat production due to the low efficiency of the anode. The x-ray emitted can be modified through flat filters within the collimator. The first filter is the glass or metal enclosed and all permanent filters inside the source, this component is named inherent filtration. Other filters can be added, depends on the procedure or protocol, usually are used copper or aluminum or together that range from 0.3 mm to 1 mm, and this process is named “beam hardening” because proportionally reduce the number of lower-energy photons so can reduce the skin exposure.

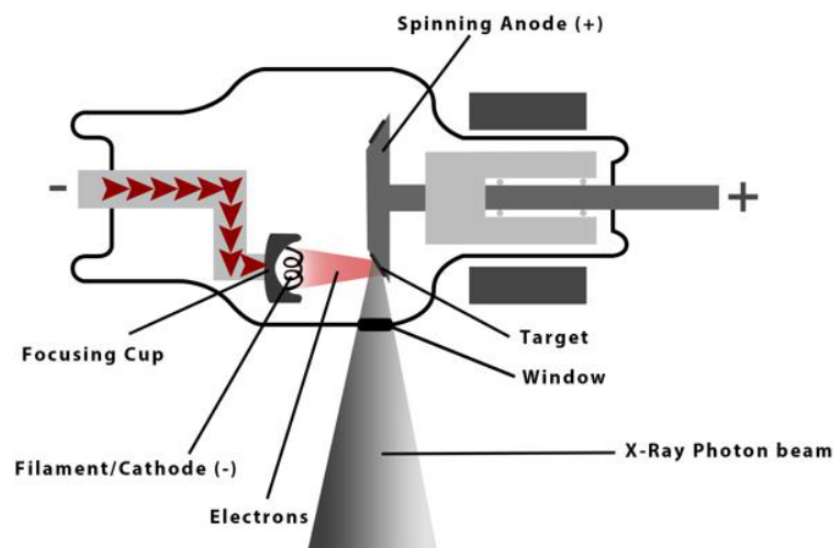


FIGURE 4.1: X-ray tube.

### 4.3 Detector

The detector is a digital flat-panel image receptor made of silicon inside a substance capable of interacting with x-ray, cesium iodide (CsI), transforming x-ray into electric current. The greater is the charge in a spot and the greater is the number of photons that hit the spot. Inside the semiconductor are placed some metallization that read the charge in a small detector area. Every pixel in the final image corresponds to metallization and the greater is the number of metallization the better is the spatial resolution of the detector. In modern fluoroscopic device is found the Automatic Dose Rate Control (ADRC), a feedback loop that through the current level of

the detector is managed the characteristic parameters of the x-ray tube (described in Appendix A) obtaining a good quality image, accounting for the changes in patient size and thickness.

## 4.4 Operating console

Generally, near the table is mounted a console from which the operator can manage the position of C-arm, procedure table, field of view (FOV), distance of the detector from the patient. Two foot pedals allow to choose the type of image (Fluoroscopy/ Stationary acquisition) and pushing the pedal can be controlled the duration of the exposure. Moreover, the same console is inside a room next to the table where the operator can protect himself from x-ray and in the same room is situated a console that communicates with the monitor and the database for pictures archiving. In the context of this project, it has been possible to work on different fluoroscope machines of different departments at the University Hospital of Innsbruck, has been used single plane and biplane Philips FD 20 (Figure 4.2), single plane and biplane Siemens Axiom Artis Zee (Figure 4.3) and Siemens Fluorospot Compact S1 (Figure 4.4). Only the last one is mobile equipment used in first aid department allowing a rapid radiological exam, instead the others are more advanced fluoroscopic equipment mostly located in operating rooms.



FIGURE 4.2: Biplane Philips FD 20.



FIGURE 4.3: Biplane Siemens Axiom Artis Zee.



FIGURE 4.4: Siemens Fluorospot Compact S1.

## Chapter 5

# Digital Imaging and Communications in Medicine (DICOM)

DICOM is a global standard that defines the criteria for communication, archiving and visualization of the data generated from medical devices (Pianykh, 2008). The functionality of the DICOM is lying in the fact that the standard itself models the real-world data such as patient information, treatment units, etc. into objects that obtain certain attributes (f.e. Patient age, sex, height, etc.) that describe the object. This object is referred to as Information Object Definition (IOD). Since all the object attributes can be dates, measures or other types, DICOM standardizes all the relevant clinical data types, which are all included into 27 basic data types, known as value representations (VR). In the Figure 5.1 is seen that each VR has its abbreviation name consisting of two letters, definition of content, allowed characters and length of data in characters. In short, the VR can be defined as a format in which all standard data attributes must be represented.

Since in the DICOM standard, there are over 2000 standard data attributes (items), the way to organize these items was to label each one with its own so called "tag". The tag represents the number dedicated to each attribute in the IOD and it is composed of two 16 bits numbers: group and element. Besides the previously mentioned data element definitions, the DICOM data dictionary also contains the value multiplicity (VM) definition, which gives information about the number of values of its type. Below, in Figure 5.2 is shown a DICOM example.

VR Name	Definition	Character Repertoire	Length of Value
SH Short String	A character string that may be padded with leading and/or trailing spaces. The character code 05CH (the BACKSLASH "\" in ISO-IR 6) shall not be present, as it is used as the delimiter between values for multiple data elements. The string shall not have Control Characters except ESC.	Default Character Repertoire and/or as defined by (0008,0005) excluding character code 5CH (the BACKSLASH "\" in ISO-IR 6) and all Control Characters except ESC when used for ISO 2022 escape sequences.	16 chars maximum (see Note in Section 6.2)
SL Signed Long	Signed binary integer 32 bits long in 2's complement form. Represents an integer, n, in the range: $-2^{31} \leq n \leq 2^{31}-1$ .	not applicable	4 bytes fixed
SQ Sequence of Items	Value is a Sequence of zero or more Items, as defined in Section 7.5.	not applicable (see Section 7.5)	not applicable (see Section 7.5)
SS Signed Short	Signed binary integer 16 bits long in 2's complement form. Represents an integer n in the range: $-2^{15} \leq n \leq 2^{15}-1$ .	not applicable	2 bytes fixed

FIGURE 5.1: Example of VM from DICOM standard.

Tag	Name	Keyword	VR	VM	
(0008,0001)	Length to End	LengthToEnd	UL	1	RET
(0008,0005)	Specific Character Set	SpecificCharacterSet	CS	1-n	
(0008,0006)	Language Code Sequence	LanguageCodeSequence	SQ	1	
(0008,0008)	Image Type	ImageType	CS	2-n	
(0008,0010)	Recognition Code	RecognitionCode	SH	1	RET
(0008,0012)	Instance Creation Date	InstanceCreationDate	DA	1	
(0008,0013)	Instance Creation Time	InstanceCreationTime	TM	1	
(0008,0014)	Instance Creator UID	InstanceCreatorUID	UI	1	
(0008,0015)	Instance Coercion DateTime	InstanceCoercionDateTime	DT	1	
(0008,0016)	SOP Class UID	SOPClassUID	UI	1	
(0008,0018)	SOP Instance UID	SOPInstanceUID	UI	1	
(0008,001A)	Related General SOP Class UID	RelatedGeneralSOPClassUID	UI	1-n	
(0008,001B)	Original Specialized SOP Class UID	OriginalSpecializedSOPClassUID	UI	1	
(0008,0020)	Study Date	StudyDate	DA	1	
(0008,0021)	Series Date	SeriesDate	DA	1	
(0008,0022)	Acquisition Date	AcquisitionDate	DA	1	

FIGURE 5.2: Example of "tag" from DICOM standard.

## 5.1 Radiation Dose Structured Report (RDSR)

In accordance with IEC 60601-2-43 2nd edition (IEC, 2010), RDSR is now required to be supported on new XA systems in order to facilitate non-proprietary access to examination data. RDSR is introduced as a part of DICOM standard since the development of the growing need to obtain and store radiation exposure relevant information during the x-ray therapy and examination. The RDSR itself consists of:

- DICOM header

- Container with dose accumulation data
- Radiation data container for each event during the procedure

RDSR represents the hierarchical structure, or in other words "the tree structure" of content data obtained from the x-ray procedure, encoded in DICOM. The structure itself can be compared with the structure of an XML file, the organization of content items is conducted in such manner that each SR has its own single "root content" in form of the document title, on which is then linked the "tree structure" that is representing the document content. In the RDSR hierarchy, it is also necessary that content items are related to each other, or in other words, each parent item must have a relationship with the child item, an example is showed below in Figure 5.3.

```

General parameter 1
:
General parameter i

Irradiation event 1:
  irradiation event parameter 1
  :
  irradiation event parameter k
:
Irradiation event j:
  irradiation event parameter 1
  :
  irradiation event parameter k.

```

---

FIGURE 5.3: Hierarchical structure of RDSR.

For a given modality (e.g., CT or XA) the DICOM standard specifies templates, a chronological list of content item containers, that should be inserted inside the RDSR and are chosen by manufacturers. For this project, since are using only the x-ray angiography (XA) modality, is introducing the template TID 10003.

"TID 10003 conveys the dose and equipment parameters of a single irradiation event and is structured to consider equipment with various levels of integration between the components (x-ray Source, Plate or Detector, and Gantry/Table) of the equipment. An irradiation event is the loading of x-ray equipment caused by a single continuous actuation of the equipment's irradiation switch, from the start of the loading time of the first pulse until the loading time trailing edge of the final pulse.

Individual Irradiation Events are described by a set of accompanying physical parameters that are sufficient to understand the "quality" of irradiation that is being applied."(Pianykh, 2008).

## Chapter 6

# Phantom

A key point of SDM to reach a good accuracy is the selection of phantom that leads to the best patient-phantom matching. Today, several possible phantom models are available on the market, such as:

- mathematical phantom
- voxel phantom
- BREP

Mathematical phantoms are the simplest form of medical phantoms, consisting of mathematical formulas, which are mimicking a human body surface. A more sophisticated or second generation phantom model is a voxel phantom, where actual patient body anatomy is represented by voxels (volumetric pixels), which are gained by the image acquisition of the patient, using the CT or MRI devices. The most sophisticated, third generation phantom model is Boundary Representation Phantom (BREP). This type of phantom is designed by the usage of polygonal mesh method or Non-Uniform Rational B-Spline (NURBS). The main advantage of BREPs compared to the voxel phantoms is availableness of broad spectrum of computerized operations which are providing the opportunity for very good geometry deformation of the phantom.

For this work, is chosen the Boundary Representation Phantom and have been generated three different phantom models. The first is a hermaphrodite phantom built using a free CAD Fusion360 allowing to build simple 3D solids (cylinder, sphere and cone) and references for dimensions are being obtained from the PCXMC (Tapiovaara and Siiskonen, 2008). According to the patient weight and total height,

some reference dimensions like trunk height, trunk thickness, trunk width (including arms and not including arms), and leg length are provided for newborns, 1 year old, 5 year old, 10 year old, 15 year old and adult patients. These phantoms have been specified by Cristy and Eckerman (1987) but later they are modified according to the real patient dimensions applying scaling factors.

TABLE 6.1: PCXMC phantom dimension.

	<b>Weight</b> (kg)	<b>Total height</b> (cm)	<b>Trunk height</b> (cm)	<b>Trunk thickness</b> (cm)	<b>Trunk width with arms</b> (cm)	<b>Trunk width armless</b> (cm)	<b>Leg length</b> (cm)
Newborn	3.40	50.9	21.6	9.8	10.94	12.7	16.8
1 year old	9.20	74.4	30.7	13.0	15.12	17.6	26.5
5 year old	19.0	109.1	40.8	15.0	19.64	22.9	48.0
10 year old	32.4	139.8	50.8	16.8	23.84	27.8	66.0
15 year old	56.3	168.1	63.1	19.6	29.66	34.5	78.0
Adult	73.2	178.6	70.0	20.0	34.40	40.0	80.0

Low matching patient-phantom is a common problem of this phantom type for its simple surface, for that reason is possible to create with specific software a more advanced phantom that provides high quality anatomical surface. For the last two BREP has been chosen to use the phantoms of the Max Hellström's project PySkinDose (Hellström, 2018) that provides four different types of gender and age (adult female, adult male, junior female, junior male). These phantoms have been modified with Fusion360 generating a new armless model so the number of phantom types rises to nine.

Moreover, with the same CAD has been upgraded phantom mesh improving the uniform distribution of surface points and allows further modification of these basic phantoms by letting the user change triangle mesh size ( $1\text{ cm}^2$ ,  $1.5\text{ cm}^2$ ,  $2\text{ cm}^2$ ).

To refine the patient-phantom matching has been considered the guideline of PCXMC project that includes scaling factors in order to resemble the actual patient more closely. Obtaining information by RDSR, concerning the mass (M) or height (h) or any of them, are used the formula below:

$$s_z = \frac{h}{h_0} \quad (6.1)$$

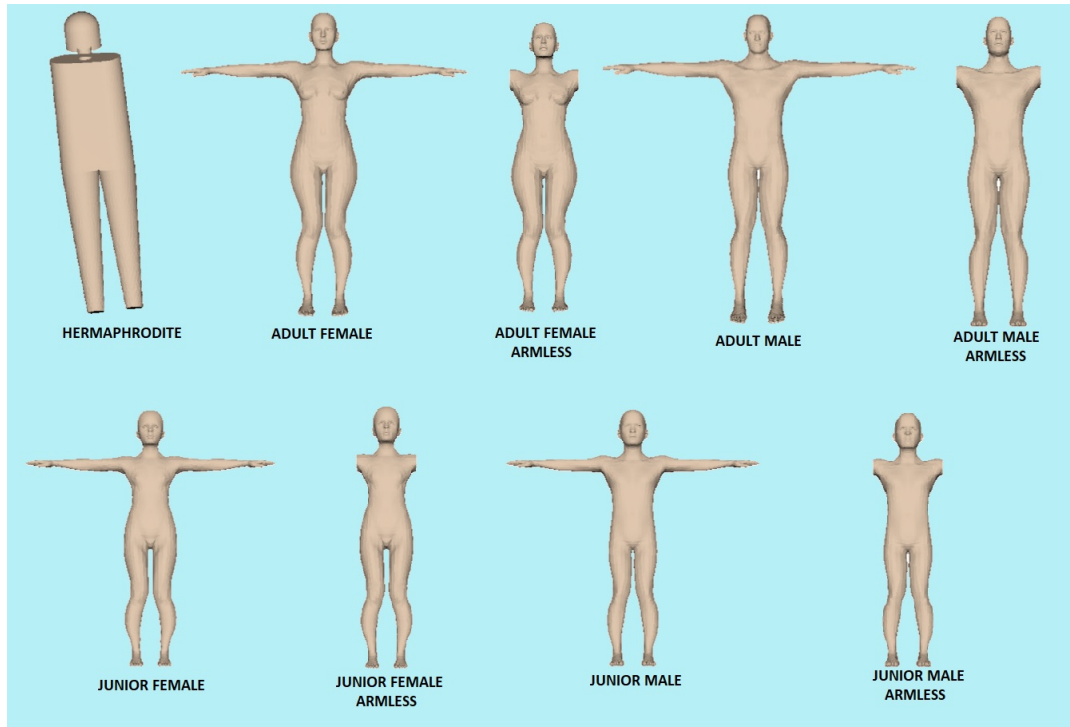


FIGURE 6.1: Phantom models for Skin Dose Map.

$$s_{xy} = \sqrt{\frac{h_0 * M}{h * M_0}} \quad (6.2)$$

where  $s_z$  is the scaling factor in the direction of the z-axis (phantom height),  $s_{xy}$  the scaling factor in the directions of the x and y-axes (phantom width and thickness, respectively), and  $h_0$  and  $M_0$  are the height and weight of the unscaled phantom. All dimensions of the phantoms are then multiplied by these scaling factors. The coordinates corresponding to the transformed phantom,  $(x, y, z)$ , are obtained from the coordinates of the same anatomical point corresponding to the basic phantom,  $(x_0, y_0, z_0)$ , by

$$\begin{aligned} x &= s_{xy}x_0 \\ y &= s_{xy}y_0 \\ z &= s_z z_0 \end{aligned} \quad (6.3)$$

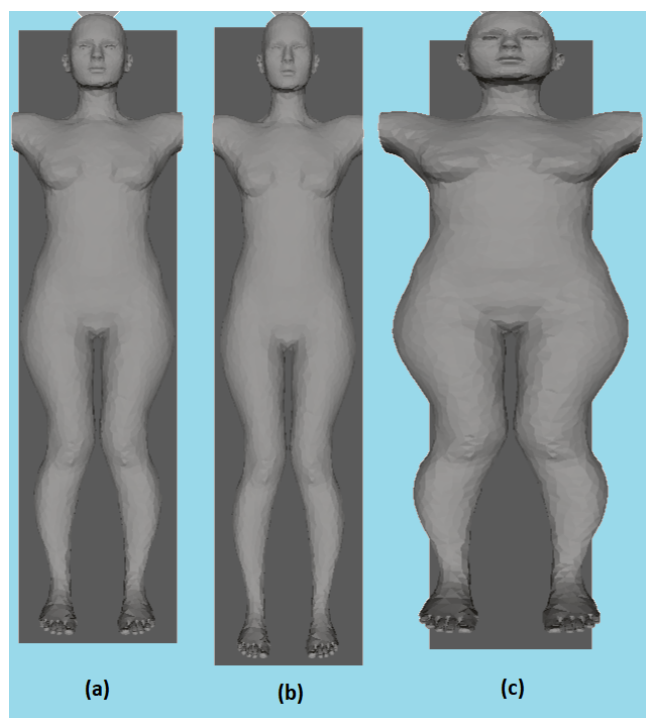


FIGURE 6.2: Frontal view of scaled adult female armless phantom.  
(a) 1.75 m/ 101 kg. (b) 2.00 m/ 101 kg. (c) 1.67 m/ 200 kg.

## Chapter 7

# Geometry

A key point of SDM is the definition of reference systems for the objects taken into consideration in 3D space. Concerning the patient, the origin is placed on head end of phantom with z-axis along the backbone toward the head, x-axis from patient right to its left and y-axis from patient front to back.

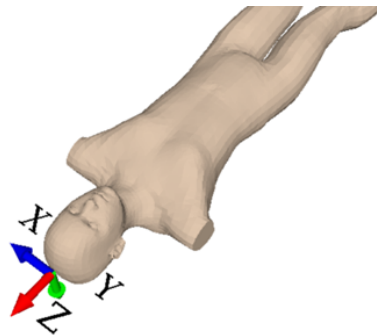


FIGURE 7.1: Phantom reference system.

Even the operating table presents same orientation of patient reference system, but the origin is translated in head end of the table and motions in x-y plane toward x and z, according to the DICOM standard, are named respectively “Table Longitudinal Direction” and “Table Lateral Direction”, y motion “Table Vertical Direction”.

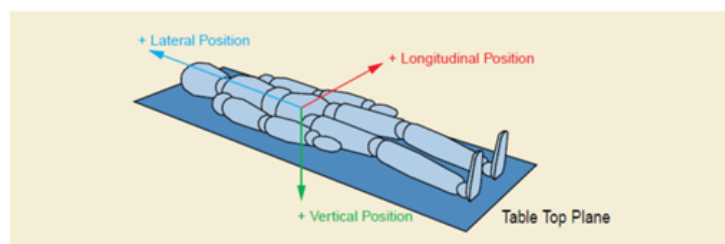


FIGURE 7.2: Operating table reference system.

To complete a description of reference systems is necessary to introduce others. The C-arm presents a rotation center named "Isocenter", not necessary in the middle of distance between source and detector, that is the origin of c-arm reference system and isocenter reference system. The first one follows c-arm rototranslation and y-axis lies on the straight line passing through source and detector, while the latter follows c-arm translation and maintains fixed axis direction. To keep the simplest possible the geometry of this work has been defined the isocenter reference system as the absolute reference system so from now on all objects in 3D space are referencing the isocenter coordinate system.

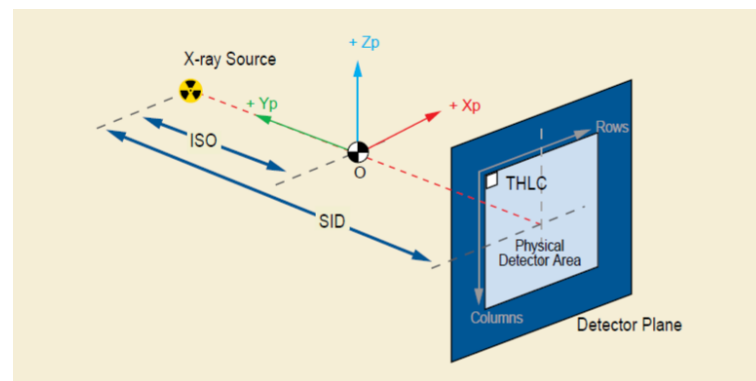


FIGURE 7.3: C-arm reference system.

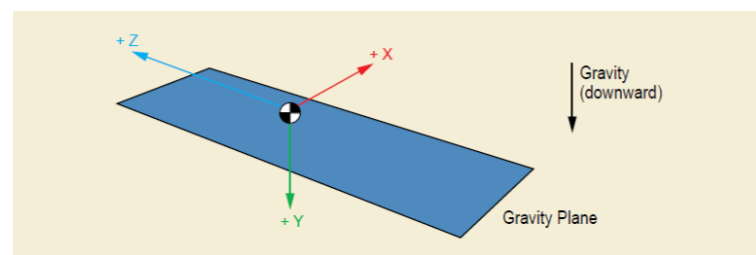


FIGURE 7.4: Isocenter reference system.

Besides the information obtained about the size and shape of the patient anatomy, to match the patient geometry during the XA intervention, also the information about the patient orientation and patient position on the table must be provided. The patient orientation parameter is obtained from the DICOM RDSR, while the exact patient position determination on the table top is much more difficult to achieve, and for this purpose, two approaches are suggested, the head-centric and target-centric approach.

The first way of patient position determination is head-centric approach, a widely used technique, which is based on predefining the distance of the patient head top (which is defined as patient origin) to the head edge of the table. During the patient position reconstruction, the medical phantom position of the head representation is calculated with the exact distance from the head edge of the table as showed in Figure 7.5. The HC approach is widely used as a standard patient positioning reconstruction method during the XA interventions.

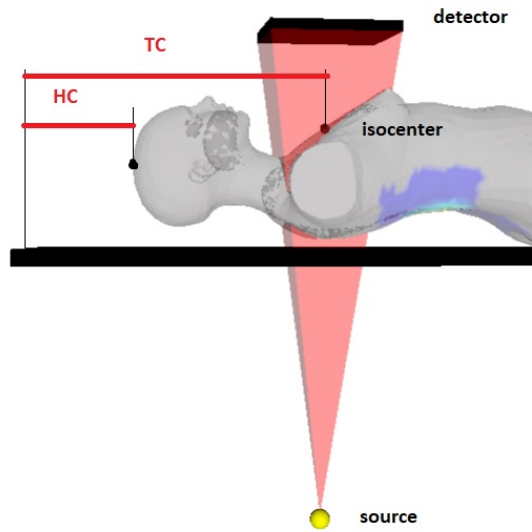


FIGURE 7.5: Patient position approaches.

In order to achieve the accuracy improvement in terms of dose calculation, the target-centric approach is proposed in study by (Omar et al., 2016). The TC technique is based on the fact that during the irradiation procedure, meaningful time is devoted to target organ visualization. Hence, the source beam isocenter position may be reconstructed in relation to the head edge of the table. By locating the median beam isocenter position, the target organ region is reconstructed. As proposed by Omar et al, the term median, instead of medium, is used since the algorithm exclude time period during the irradiation event, when the geometry is not aimed to visualize the target region as displayed below:

$$r_{target}^{TC} = \sum_{i \in x,y,z} \text{median}(r_{iso}(t) * e_i | t \in \mathcal{X}) e_i \quad (7.1)$$

Where:

- $r_{iso}(t) = (x,y,z)$  represent the source isocenter position in relation to the head end of the table during the time of irradiation (t)
- $e_i = (e_x, e_y, e_z)$  represent vectors that form standard basis

TC approach provides a more precise detection of the target organ region, since, opposite to HC, which is based on assumption that target organ position is approximately located on certain distance from head origin with slight deviation tolerance, the TC is calculating the distance from table head end to isocenter which is taken as indicator of the target organ location, without relying on the distance from head origin to target region assumptions.

## Chapter 8

# Parameters

Before to start explaining the whole project is necessary to stop and discuss parameters extracted by RDSR. The DICOM Conformance Statement is a document produced by device manufacturers that provides specific information about used templates and parameters. Since this document differs for every manufacturer, has been analyzed for every machine and has been found differences in some parameters or even the lack of others. The parameters are divided into two table: in Table 8.1 general information present in all RDSR and in Table 8.2 are shown event-related parameters. All parameters are described in Appendix A.

TABLE 8.1: List of general parameters

Name	Tag	VR
StudyDate	0008,0020	DA
Manufacturer	0008,0070	LO
StationName	0008,1010	SH
StudyDescription	0008,1030	LO
ManufacturerModelName	0008,1090	LO
PatientName	0010,0010	PN
PatientID	0010,0020	LO
PatientSex	0010,0040	CS
PatientAge	0010,1010	AS
PatientSize	0010,1020	DS
PatientWeight	0010,1030	DS
DeviceSerialNumber	0018,1000	LO
StudyInstanceUID	0020,000d	UI

TABLE 8.2: List of specific parameters per event

Parameter	(Context Group ID; CID) RDSR Concept Name	Manufacturer
Table position ( $x$ )	(113751) Table Longitudinal Position	Philips and Siemens
Table position ( $y$ )	(113753/021) Table Height Position	Philips and Siemens
Table position ( $z$ )	(113752) Table Lateral Position	Philips and Siemens
Source to Isocenter Distance (SID)	(113748) Distance Source to Isocenter	Philips and Siemens
C-arm RAO–LAO rotation ( $a$ )	(112011) Positioner Primary Angle	Philips and Siemens
C-arm CAU–CRA rotation ( $b$ )	(112012) Positioner Secondary Angle	Philips and Siemens
Exposure	(113736) Exposure	Siemens
Tube kilovoltage	(113733) KVP	Philips and Siemens
Filter type	(113772) X-Ray Filter Type	Philips and Siemens
Filter material	(113757) X-Ray Filter Material	Philips and Siemens
Filter thickness min	(113758) X-Ray Filter Thickness Minimum	Philips and Siemens
Filter thickness max	(113773) X-Ray Filter Thickness Maximum	Philips and Siemens
Acquisition plane	(113764) Acquisition Plane	Philips and Siemens
Event type	(113721) Irradiation Event Type	Philips and Siemens
Interventional Reference Point (IRP)	(113780) Reference Point Definition	Philips and Siemens
Dose Area Product (DAP)	(122130) Dose Area Product	Philips and Siemens
Reference Air Kerma Value	(113738) Dose (RP)	Philips and Siemens
Tube current	(113734) X-Ray Tube Current	Philips and Siemens
Source to Detector Distance (SDD)	(113750) Distance Source to Detector	Philips and Siemens
Target	(123014) Target Region	Philips and Siemens
Height of system	(001) Height of System	Philips
Patient table relationship	(113745) Patient Table Relationship	Philips
Patient orientation	(113743) Patient Orientation	Philips
Patient orientation modifier	(113744) Patient Orientation Modifier	Philips
Shutter dimension	(005) Wedges and Shutters	Philips
Longitudinal beam	(015) Longitudinal Beam Position	Philips
Pulse width	(113793) Pulse Width	Philips and Siemens
Pulses number	(113768) Number of Pulses	Philips and Siemens

## Chapter 9

# Absorbed dose calculation

In order to determine radiation exposure incident on the body surface, utilizing the data extracted from the DICOM RDSR, the most convenient way to achieve desired result is the usage of Reference Air Kerma ( $K_{air,ref}$ ) or in other words kerma free-in-air. The accumulated Air Kerma is calculated at the IRP for all projection angles, independent of where on the patient the irradiation has been deposited. This is a standard method used by all systems that causes the accumulated air Kerma to correspond to the unusual and worst scenario: all irradiations have been deposited to the same skin surface during procedures. This is not always the case, since the staff might choose different projection angles when suitable for the procedure and might lead to an absorbed dose distribution that includes overlapping irradiated areas. Moreover, since the Reference Air Kerma gives information only about the dose in the reference point, 15 cm toward x-ray source from isocenter for the standard IEC 60601-2-43, is necessary to convert this measure in order to calculate the right value in a specific skin point that might be at different distance. Introducing the multiplicative correction factors is possible to estimate absorbed skin dose  $D_{skin}$ :

$$D_{skin} = (K_{air,IRP})_a \prod_i k_i \quad (9.1)$$

Where  $k_i$  corrects for the i-th factor that differentiates  $D_{skin}$  from  $(K_{air,IRP})_a$ .

### 9.1 Reference Air Kerma

The use of air kerma for the determination of dosimetry quantities in diagnostic radiology is well established and consistent with ICRU74 (ICRU, 2005) and the IAEA

TRS-457 code of practice (IAEA, 2007). On every radiological system is mounted an ionization chamber providing the Air Kerma Value at IRP with allowed deviation of  $\pm 35\%$  for IEC and FDA. The Kerma is the acronym for Kinetic Energy Released per unit Mass and is a non-stochastic quantity, related to the energy transferred from uncharged particles to matter. It is defined as the quotient  $dE_{tr}$  by  $dm$ , where  $dE_{tr}$  is the sum of the initial kinetic energies of all the charged particles liberated by uncharged particles in a mass  $dm$  of material:

$$K = \frac{dE_{tr}}{dm} \quad (9.2)$$

In diagnostic radiology, for a given material and radiation field, the kerma and absorbed dose are numerically equal when charged particle equilibrium (CPE) is established. CPE exists for the volume  $v$ , enclosed by a larger region  $V$  consisting of the same material as  $v$ , if each charged particle of a given type and energy leaving  $v$  is replaced by an identical particle of the same energy entering. Since skin is the interface between patient body and other mediums like air or table pad, CPE is not strictly fulfilled for skin dose calculations. But assuming that changes in photon fluence are small, and the volume of interest has small dimensions compared to the electron range is possible to approximate the CPE.

## 9.2 Correction source to skin distance

During a procedure, the operator might move the C-arm around patient and at the same time the reference point could be far from skin (Figure 9.1). Since is unusual that x-ray beam hits skin at the reference point, the Reference Air Kerma value taken from RDSR need to be corrected at every movement of C-arm.

In the case where  $SSD \neq d_{IRP}$ , then the ratio between air Kerma at the skin surface and the air Kerma at IRP is given by

$$\frac{K_{a,SSD}}{K_{a,IRP}} = \frac{\phi_{SSD}}{\phi_{IRP}} = \left( \frac{d_{IRP}}{SSD} \right)^2 \quad (9.3)$$

according to the inverse-square-law (isq) photon fluence distance scaling. Where  $d_{IRP}$  is the distance from source to IRP and SSD is the distance from source to skin.

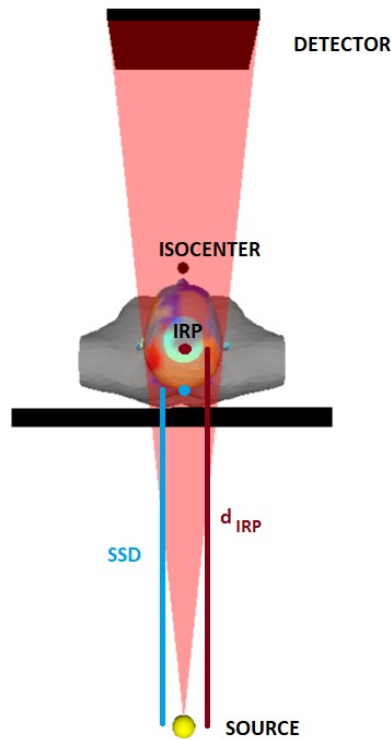


FIGURE 9.1: Transverse view of IR equipment.

From (9.3) is possible to extract the inverse-square-law correction factor:

$$k_{isq} = \left( \frac{d_{IRP}}{SSD} \right)^2 \quad (9.4)$$

### 9.3 Backscatter factor

In diagnostic radiology, backscattered photons due to Compton scattering in the patient can contribute to a substantial fraction of the absorbed skin dose. It is known that the backscatter factor (BSF) depends on the x-ray spectrum, the field geometry, the dimension of the phantom and its material. The BSF is defined as the ratio of the air kerma on the surface of a phantom to the air kerma free-in-air, in the same point in space in the absence of the phantom. This definition in the case of a water phantom was adopted, for example by the IAEA code of practice. By approximating the body of the patient as purely water equivalent, the correction equals

$$k_{BS} = \frac{(K_{a,SSD})_w}{(K_{a,SSD})_a} \quad (9.5)$$

The calculation of the BSF is carried out using Monte Carlo methods and mathematical phantoms of a rectangular shape with a homogeneous material composition of water, ICRU tissue or PMMA (Petoussi-Henss et al., 1998; Benmakhoulouf et al., 2011), but for this work has been taken tabulated values from PySkinDose project.

The values have been obtained by Monte Carlo simulation with kVp ranging from 50 kV to 150 kV for square field sizes (FS) (5, 10, 20, 25, 35)  $cm^2$  and a (15 x 30 x 30)  $cm^3$  water phantom. The data have been interpolated as a function of kVp, HVL and field size.

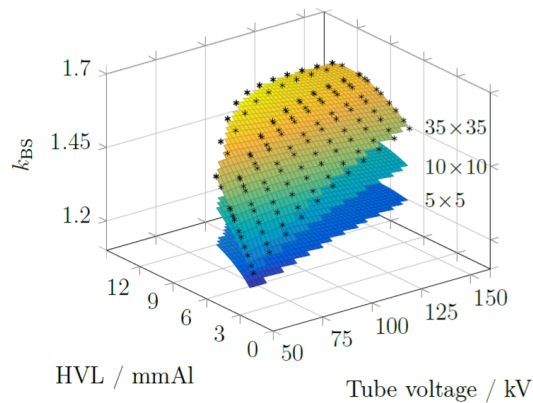


FIGURE 9.2: Interpolation of MC simulated data for BSF.

## 9.4 Correction from air kerma to skin kerma

Starting from a different definition of kerma, is introducing the mass energy absorption coefficient. The kerma is the sum of collision kerma and radiative kerma.

$$K = K_{rad} + K_{col} \quad (9.6)$$

Collision kerma ( $K_{col}$ ) is related to the part of the kinetic energy of the secondary charged particles which is spent in collisions, resulting in ionization and excitation of atoms in matter. Instead, radiative kerma ( $K_{rad}$ ) is related to the portion of the initial kinetic energy of the secondary charged particles which is converted into photon energy. Consequently, the kerma and the collision kerma can be expressed by

$$K = \phi h\nu \left( \frac{\mu_{tr}}{\rho} \right) = \left( \frac{\mu_{tr}}{\rho} \right) \psi \quad (9.7)$$

$$K_{col} = \phi h\nu \left( \frac{\mu_{en}}{\rho} \right) = \left( \frac{\mu_{en}}{\rho} \right) \psi \quad (9.8)$$

- $\left( \frac{\mu_{tr}}{\rho} \right)$  : mass energy transfer coefficient
- $\psi$  : energy fluence
- $\left( \frac{\mu_{en}}{\rho} \right)$  : mass energy absorption coefficient

From the relationship between kerma and collision kerma

$$K_{col} = K(1 - g) \quad (9.9)$$

where  $g$  is the energy fraction lost to radiative processes and assuming this variable as zero in diagnostic radiology, is obtained the relationship

$$\left( \frac{\mu_{tr}}{\rho} \right) = \left( \frac{\mu_{en}}{\rho} \right) \quad (9.10)$$

Since human tissue is assumed to be water equivalent like in backscatter factor simulation, the conversion from air kerma to skin kerma results in the medium correction factor

$$k_{med} = \frac{(\mu_{en}/\rho)_{skin}}{(\mu_{en}/\rho)_{air}} = \left( \frac{\mu_{en}}{\rho} \right)_{air}^{water} \quad (9.11)$$

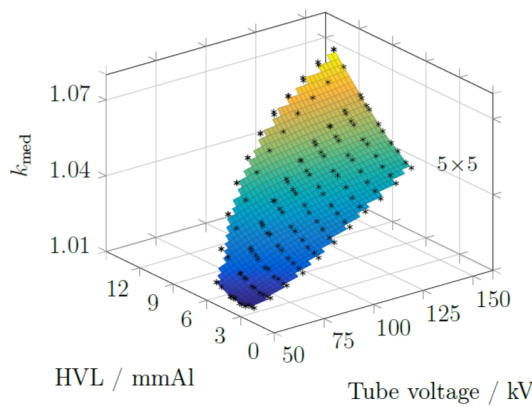


FIGURE 9.3: Interpolation of MC simulated data for  $k_{med}$ .

The values have been obtained by Monte Carlo simulation with kVp ranging from 50 kV to 150 kV for square field sizes (FS) (5, 10, 20, 25, 35)  $cm^2$  and a (15 x 30 x 30)  $cm^3$  water phantom. The data have been interpolated as a function of kVp, HVL

and field size, but has a negligible field size dependency. Even for this correction factor have been taken the values from PySkinDose project.

## 9.5 Correction for patient support table

For every projection where the patient support table and pad are located between the x-ray tube and the patient, skin dose calculations need to be corrected for attenuation of the photon fluence and photon scattering in the table and pad. The approach to measure the combined effect of the table and pad with normal incidence under-table projection, including both attenuation and forward scattering, is obtained by measuring the air Kerma with and without the table and pad blocking the beam. The point of measurement should be located directly above the tabletop, in order to include clinically relevant forward scatter. This results in the table and pad correction factor

$$k_{(T+P)} = \frac{(K_{a,IRP})_{T+P}}{(K_{a,IRP})_a} \quad (9.12)$$

The correction factor is picked up with x-ray tube perpendicular to table, for kVp ranging from 50 kV to 150 kV and Aluminium and Copper filters ranging from 0 mm to 1 mm. For this work has been taken tabulated values from PySkinDose project.

## 9.6 Summary of correction factor

Before using (9.13) for the skin absorbed dose is necessary to read the air kerma value of every event and calculate the correction factors for the skin points inside irradiated area.

$$\begin{aligned} D_{skin} &= (K_{air,IRP})_a \prod_i k_i = \\ &= (K_{air,IRP})_a k_{isq} k_{bs} k_{med} k_{(T+P)} = \\ &= (K_{air,IRP})_a \left( \frac{d_{IRP}}{SSD} \right)^2 k_{bs} k_{med} k_{(T+P)} \end{aligned} \quad (9.13)$$

The final step to evaluate the Peak Skin Dose (PSD) value is the dose summation for overlapping skin points.



---

FIGURE 9.4: Experiment for the extrapolation of  $k_{(T+P)}$  (Hellström, 2018).



## Chapter 10

# Environment setup

The software module developed in this project, is based on Linux platform, running on Ubuntu 18.04 LTS operating system. For the development purpose of the application designed in this project, the Code::Blocks IDE version 16.01 is chosen, due to its simplicity and application lightweight. The GNU GCC compiler has been chosen, which is following the C++11 ISO standard. Since the dose estimation monitoring system is based on data extracted from RDSRs, the DCMTK library is chosen to enable the data extraction. Since the software has been developed for the server of Innsbruck Hospital, visualization of output has been realized with cgi.h, a C library, and javascript and has been necessary to install Apache Web Server to use the Hospital server.



## Chapter 11

# Software information and architecture

In this section is showing up characteristics and architecture of the software obtaining the rendering in web page and archiving new data in a default path. The software has been programmed to work completely automatic from the web page or command line. To run the main code is necessary to insert the chosen phantom and DICOM file as arguments. Later five personal libraries are automatically called by the main generating the needed data (ascii and X3D files) that will be used by web page for the visualization of the skin dose map. In Figure 11.1 is showed the flowchart of the whole software.

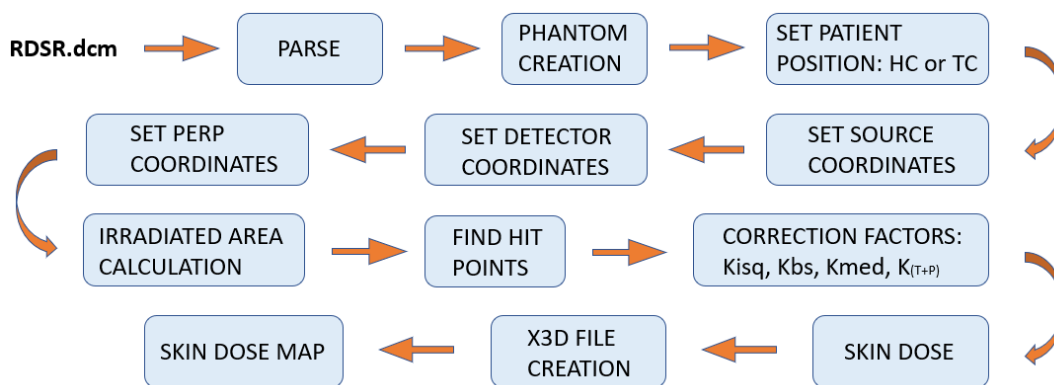


FIGURE 11.1: Flowchart of Skin Dose Map calculation.

Regarding archiving has been chosen to organize a hierarchical storage firstly based on the examination date and after on StudyInstanceUID, different for each examination. The generated folder includes:

- *info.txt*: contains patient and exam information
- *skinDose.txt*: list of points absorbed dose of phantom
- *output.txt*: StudyDate, StudyInstanceUID, max peak skin dose and any errors that occurs during the execution
- *colors.txt*: list of points color of phantom
- *colorbar.txt*: html code for the colorbar
- *event\_points.txt*: list of phantom points per event
- *geometry.txt*: all parameters for geometry reconstruction
- *event\_dose.txt*: list of points absorbed dose of phantom per event
- *Dose.txt*: list of mean absorbed dose per event
- *Skin.x3d*: file containing points and triangulation of the phantom

For the explanation of the whole project is necessary to divide itself in two parts: elaboration and visualization (chapter 13). Concerning the elaboration part, is allowed from command line to choose different configurations before the calculation:

- 3 different phantom model: geometric, standard and armless
- 3 different mesh resolution: fine, medium and rough

Otherwise, after the visualization from web page is possible to modify more parameters than before:

- patient information (age, sex, size, weight)
- patient position (HC or TC)
- phantom model
- mesh resolution

Clicking a button will be run again the main code with the new configuration.

Moreover, is possible to omit the mesh resolution allowing the software to choose automatically calibrated resolution in order to obtain fast code execution. Obviously, better is resolution and longer is execution. Since searching points of phantom is per event, large number of events corresponds longer execution. The software is developed inside a virtual machine in a PC with Intel Core i7 8th generation and 16 Gb RAM. This configuration allows to execute the software for an examination with 395 events and a rough resolution in 239 seconds, instead an examination of 81 events and a fine resolution in 472 seconds. From these data is easy to observe the close relation between number of events, mesh resolution and time consuming.



## Chapter 12

# Libraries description

In this chapter, are introducing the five libraries created to carry out the fundamental steps of the previous flow chart. The libraries have been divided grouping functions with the same context and purpose.

### 12.1 RDSRparse.h

In this library is used the DICOM Toolkit (dcmTk) to read and parse the DICOM (.dcm) files. The function “void Parameters::calcParameters(string inFile)” allows to pick up the parameters from the Radiation Dose Structured Report (RDSR) with proper item or CID. It is also possible to find the observed region of the body (head, heart, chest or entire body) and in case of heart or head is automatically used the TC approach, otherwise is checked the device serial number identifying the hospital department and selecting the heart as target only for cardiological department, while for others is selected HC approach.

All but some parameters (device model, study date, patient id, gender, age, weight, height) are stored in vectors where each cell represents an irradiation event of the RDSR and the parameters are converted in centimetres (cm), seconds (s), Gray (Gy) and degrees.

The GET functions allows to get all parameters parsed by this library, as showed in Figure 12.1.

```

string getStudyDate();
string getPatientID();
char getGender();
int getAge();
float getHeight();
float getWeight();
vector<double> getRefAirKerma();
vector<double> getDoseAreaProduct();

```

FIGURE 12.1: Example of GET functions in RDSRparse.h.

## 12.2 PatientBeamAlignmentGeometry.h

The current library is built to calculate the coordinates of the patient, referenced to the head end of the table, and the geometries of machine's C-arm. All these geometries have the same reference system with origin in the isocenter, the rotation centre of the C-arm.

Since the patient position can be set manually or automatically, have been created a function for HC approach where are set the coordinates of phantom head and a function for TC approach in which is used the formula (7.1) to automatically search the target. After, a series of functions produce the coordinates of source, detector, IRP and vertices of irradiated field at IRP.

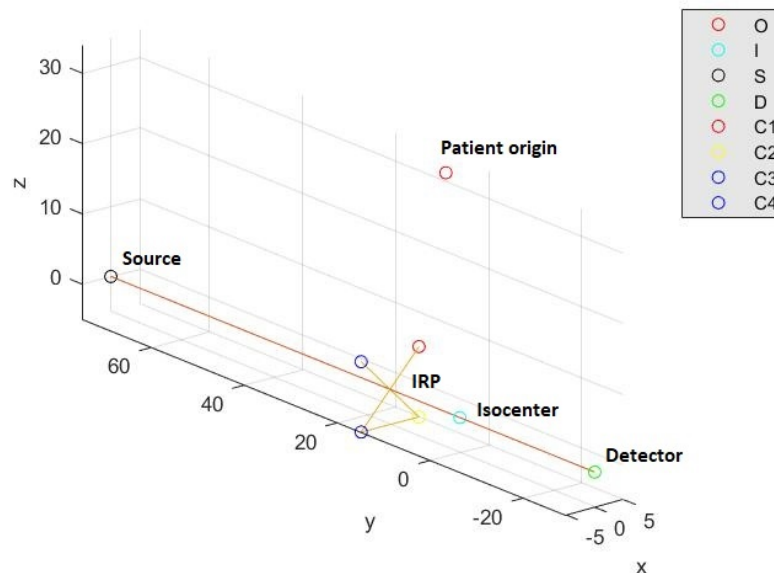


FIGURE 12.2: System coordinates representation.

## 12.3 SurfaceXRay.h

In this library are contained the functions concern phantom. The function “void SurfaceXRay:: createPhantom(…)” loads points and triangulation of the selected phantom model from ascii files (.txt) and after scaled obtaining real patient size. Knowing the selected model and the resolution, is automatically chosen the phantom with right gender and age (junior or adult).

Since the patient can lay down in the table in different position (supine or prone, head first or feet first), the function “vector<vector<vector<double>>> SurfaceXRay:: RotoTranslate(…)” allows to rotate and translate the phantom according to RDSR information.

Finally, is also included a function to search the hit points of phantom inside the pyramid generated by rectangular shape collimator that, according to the geometry information from RDSR, is possible to reconstruct the C-arm movements in relation to table for every event. This is the crucial part of the software because merges all objects with the same reference system relating each other with a series of geometrical parameters analysed in previous step.

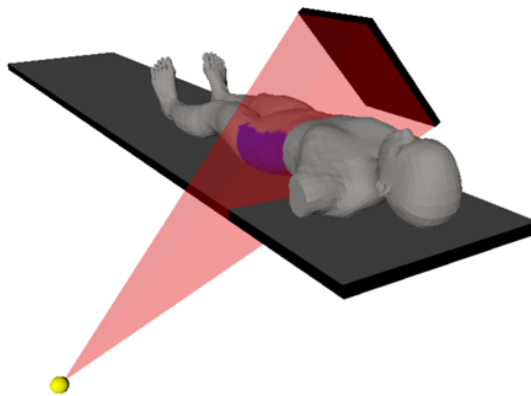


FIGURE 12.3: Example of RDSR x-ray event.

## 12.4 DSRreports.h

In this library are contained the functions concern radiation dose. Have been realized functions for the estimation of the correction factors:

- “void DSRreports::calculateKisq(...)”: gets the inverse-square-law correction factor from formula (9.4)
- “void DSRreports::calculateKbs(...)”: gets the backscatter correction factor from interpolated coefficients, obtained by different Monte Carlo simulations, multiplied by the kilovoltage (tKV), the half value layer (hvl) and field side length (fsl)
- “void DSRreports::calculateK\_med(...)”: gets the medium correction factor from Monte Carlo simulated values stored in a ascii file
- “void DSRreports::calculateKtab(...)”: gets the table and pad correction factor from a list of measured values for different condition stored in a ascii file

Since the backscatter correction factor and the medium correction factor depend on Half Value Layer (HVL), has been written a function that loads a table stored in a ascii file where is tabulated HVL for different combination of kilovoltage (kVp), Copper filtration thickness (filtration\_Cu), Aluminium filtration thickness (filtration\_Al), device model (Device), acquisition plane (Plane).

Introducing last function “void DSRreports::calculateSkinDose(...)”, is calculated the absorbed dose using formula (9.14) getting skin points and correction factors per event from previous step. After that, “vector<vector<double>> DSRreports:: getSkinDose(...)” sums up the previous results evaluating the overlapping fields and stores the absorbed dose of every skin points in a 3D vector.

## 12.5 HTML.h

The last library is a bridge between C++ and javascript because allows to store important data in ascii files to be used as variables in javascript. First step is collection of main information, as patient information and absorbed dose, in a struct with “VALUE HTML:: saveStruct(...)”. Moreover, the function “void HTML:: showStruct(VALUE valore)” shows data of the struct in a table. After are stored the data in default ascii files by “void HTML:: createHTML(VALUE valori)”. Moreover, in the same function has been implemented a routine for automatic colour code scale with

RGB codification dividing the absorbed dose in 10 levels, using 4 different colours per level with a total of 40 shade from blue to red.



## Chapter 13

# Visualization

In this chapter is talking about the web page and its characteristics, giving information about data illustrated in the Figure 13.1.

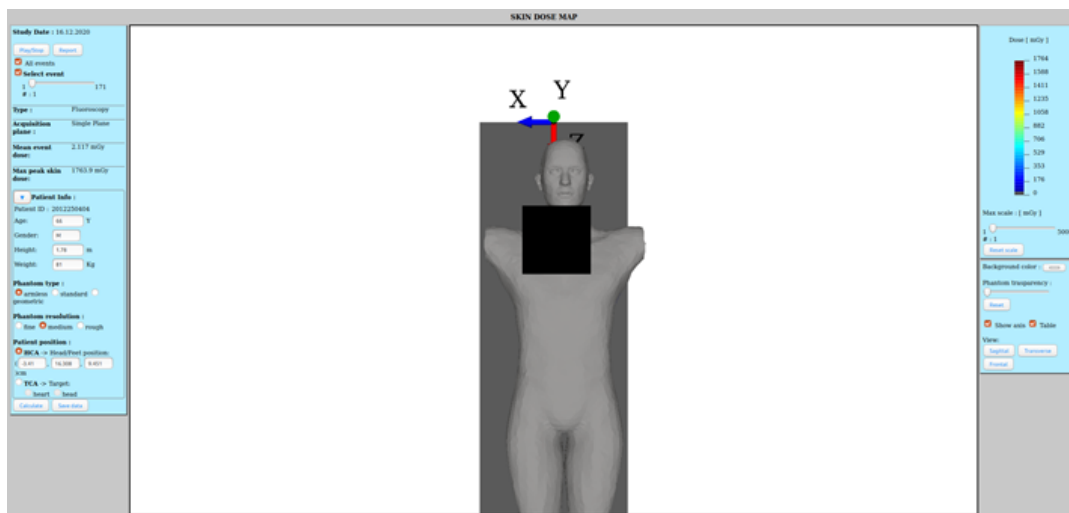
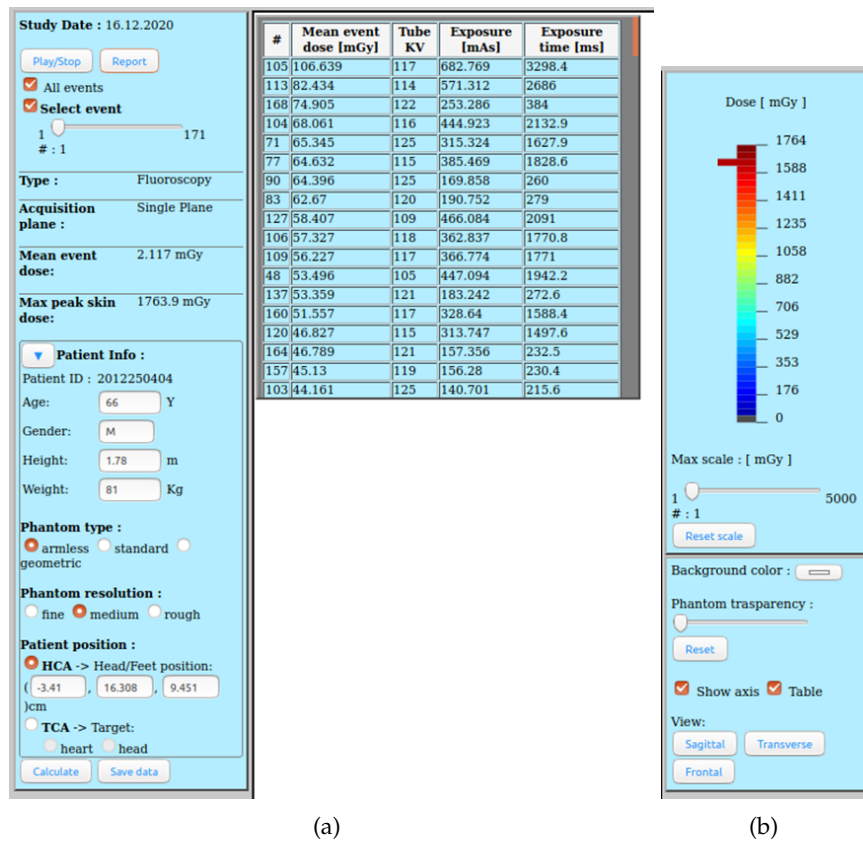


FIGURE 13.1: Web page Skin Dose Map.

The web page has been built through `cgic.h` that is an ANSI C-language library for the creation of CGI-based World Wide Web applications. This library has allowed to create a dynamical web page where automatically chooses the folder with right study date and study instance UID of the examination. When a user login in the web server is generated a temporary folder, where are stored all examination viewed in order to not affect the database. As is showed in Figure 13.1, the page has been divided in three areas: lateral columns and rendering area. Inside the rendering area is possible to navigate in the 3D space using the mouse, moving the mouse with left clicked rotates objects around the centre of rotation, imposed by double left click, and right click to zoom. Starting from left column (Figure 13.2.a), the first part

shows the parameters extracted from RDSR while the latter introduces patient info, phantom model and patient position. The “Play/Stop” button enables the visualization of C-arm movements in the examination through the rendering area. Instead, the “Report” button shows a table with x-ray tube parameters (tube kV, exposure, exposure time) in descend order beginning from the larger mean absorbed dose per event. The “All events” checkbox allows the visualization of current irradiated area in the phantom with single event absorbed dose. From slider is managed the current event to be showed on rendering area, selecting “Select event” checkbox disables the slider and moves away the C-arm from phantom. Below a table shows event type, acquisition plane, mean event dose that change moving the slider and finally the max peak skin dose. In the second half is possible to modify the current phantom configuration (phantom type and resolution), patient information and patient position. After the first elaboration, the user can improve the result checking data concerning patient information or improving the phantom position using HC or TC approach. Since the HC approach is a manual phantom positioning, is possible to insert the coordinates of phantom head from the origin showed in Figure 13.3 moving in real-time the phantom. Finally, through “Calculate” button is automatically run the software with new inputs and after the elaboration is showed the last result. If is clicked the “Save data” button the last files in temporary folder overwrite the previous in the database.

Concerning the right column (Figure 13.2.b), the colorbar can be rescaled modifying the maximum value with the slider below ranging from 1 to 5000 mGy and clicking the “Reset scale” button returns default scale. Moreover, the coloured rectangle in the colorbar represents the colour of clicked phantom point. Last part of the column groups the navigation tools changing some parameter from rendering area. Clicking on “Background color” can be chosen the colour of rendering area, while the slider modifies the phantom transparency. Instead, “Reset” button restores the default background colour and phantom transparency. The checkboxes allow the vision of axis for HC and the operating table from the rendering area. The buttons below allow to choose three different anatomical planes for view: sagittal (Figure 13.3.a), frontal (Figure 13.3.b) and transverse (Figure 13.3.c).



(a)

(b)

FIGURE 13.2: (a) Left column of SDM. (b) Right column of SDM.

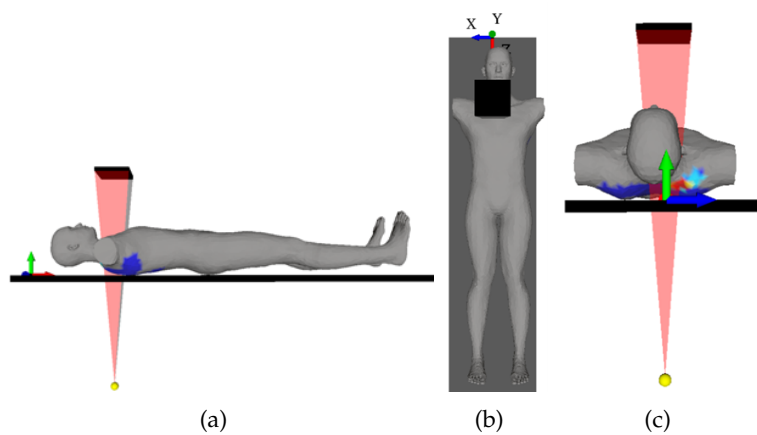


FIGURE 13.3: (a) View of lateral plane. (b) View of frontal plane. (c) View of transverse plane.



## Chapter 14

# Test and results

On 23 October 2020, the software was tested in radiological department of Innsbruck Hospital with Philips FD20 single plane device. The test was executed on Alderson Radiation Therapy (ART) phantom, an anthropomorphic phantom molded of tissue-equivalent material and follows ICRU-44 standards. The male ART represents a 175 cm tall and 73.5 kg male. The ART phantom is transected-horizontally into 2.5 cm thick slices. Each slice has holes which are plugged with bone-equivalent, soft-tissue-equivalent or lung tissue equivalent pins which can be replaced by TLD holder pins.

For skin absorbed dose test were used thermoluminescent dosimeters (TLD) placed in the thoracic area of the back in grid shape with 8 rows and 15 columns, spaced apart 2 cm, for a total of 120 TLDs.



FIGURE 14.1: TLDs placement from slice 12th to 19th of phantom.

TLD is based on the observation that many insulating crystals, when exposed

to ionizing radiation, store some of absorbed energy, which is later released as light when the crystals are heated to a few hundred degrees Celsius. The amount of light emitted can be measured and used to determine the amount of radiation that was absorbed. This phenomenon of emitting light when heated is called thermoluminescence. It is closely related to phosphorescence where light is emitted slowly at room temperature. Heating accelerates the emission of the stored energy. TLD is quite reliable and an accuracy of 3-10%. In addition, TLD has a large useful range, it can measure radiation from 0.1 Gy to much greater than the dangerous dose (5 to 10 Gy) (Cameron, 1991).

After TLDs placement, the phantom was placed supine and head first orientation. In addition, two rules, x-ray visible, were positioned on the phantom in order to get the phantom position for HC approach and irradiated area position (Figure 14.3.a).



FIGURE 14.2: Setup for test.

Concerning the examination, was selected a standard protocol for adult with abdomen as target region. In Figure 14.4 is showed a partial table with the main parameter from RDSR.

After the examination, three TLDs were placed on the table pad instead of phantom with a RaySafe Xi detector and the C-arm perpendicular to table in order to

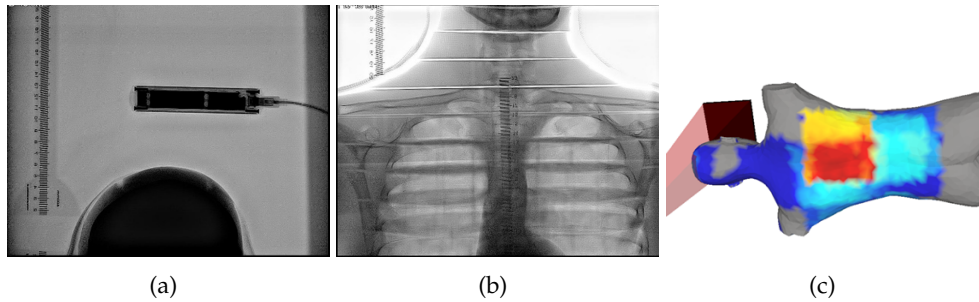


FIGURE 14.3: (a) Radiography of head and RaySafe Xi detector. (b) Chest radiography of phantom. (c) Skin dose map.

#	Type	a	b	Thet	Tlat	Tlong	sdd	sid	l_Beam	Klirp[mGy]	Dose [mGy]	Plane
1	Stationary Acquisition	0.1	-0.2	18.00	11.19	-1.18	119.4	81.0	212.3	0.409	0.405	Single Plane
2	Stationary Acquisition	0.1	-0.2	18.00	11.19	-1.18	119.4	81.0	212.3	0.034	0.033	Single Plane
3	Fluoroscopy	0.1	-0.2	18.00	11.19	-1.18	120.0	81.0	212.3	0.011	0.012	Single Plane
4	Fluoroscopy	0.1	-0.2	18.00	12.79	-1.18	120.0	81.0	210.7	0.002	0.002	Single Plane
5	Fluoroscopy	0.1	-0.2	18.00	12.79	-1.18	95.7	81.0	210.7	0.005	0.005	Single Plane
6	Fluoroscopy	0.1	-0.2	18.00	42.29	-1.18	120.0	81.0	181.2	0.016	0.021	Single Plane
7	Stationary Acquisition	0.1	-0.2	18.00	42.29	-1.18	95.7	81.0	181.2	0.152	0.191	Single Plane
8	Fluoroscopy	0.1	-0.2	18.00	42.29	-1.18	95.7	81.0	181.2	0.016	0.021	Single Plane
9	Fluoroscopy	0.1	-0.2	18.00	62.89	-1.07	95.7	81.0	168.2	0.046	0.057	Single Plane
10	Fluoroscopy	0.1	-0.2	18.00	62.89	-1.07	120.0	81.0	168.2	0.064	0.080	Single Plane
11	Stationary Acquisition	0.1	-0.2	18.00	62.89	-1.07	95.7	81.0	168.2	0.337	0.398	Single Plane
12	Fluoroscopy	0.1	-0.2	18.00	62.89	-1.07	95.7	81.0	168.2	0.039	0.049	Single Plane
13	Fluoroscopy	0.1	-16.5	18.00	62.89	-1.07	106.0	81.0	168.2	0.312	0.400	Single Plane
14	Stationary Acquisition	0.1	-16.5	18.00	62.89	-1.07	106.0	81.0	168.2	0.533	0.646	Single Plane
15	Fluoroscopy	0.1	13.4	18.00	62.89	-1.07	106.0	81.0	168.2	0.184	0.234	Single Plane
16	Stationary Acquisition	0.1	13.4	18.00	62.89	-1.07	106.0	81.0	168.2	0.468	0.567	Single Plane
17	Fluoroscopy	29.7	-1.5	18.00	62.89	-1.07	120.0	81.0	168.2	0.303	0.384	Single Plane
18	Stationary Acquisition	29.7	-1.5	18.00	62.89	-1.07	106.0	81.0	168.2	0.498	0.599	Single Plane
19	Fluoroscopy	29.7	-1.5	18.00	62.89	-1.07	120.0	81.0	168.2	0.250	0.317	Single Plane
20	Stationary Acquisition	29.7	-1.5	18.00	62.89	-1.07	106.0	81.0	168.2	0.491	0.591	Single Plane

FIGURE 14.4: Example of software output in *output.txt*.

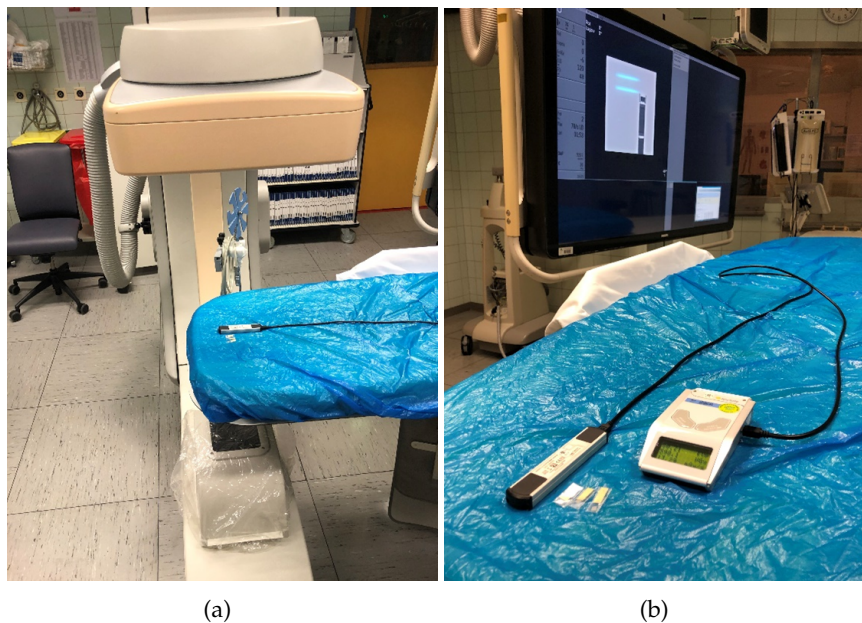


FIGURE 14.5: (a) TLDs test. (b) Setup for TLDs test.

irradiate these objects. This setup allows to check if the TLD readout corresponds to real absorbed dose.

For ten times were irradiated the objects, each time saving the detector readout.

TABLE 14.1: Results of TLDs test

Label	Detector dose [mGy]	TLD dose [mGy]	Percentage difference
d2_C05	1,149	1,525	33%
d2_C12	1,149	1,496	30%
d1_I10	1,149	1,502	31%

Table 14.1 shows that TLDs readouts present a mean percentage difference of 31.2% from total detector dose. From this value is already known that the test presents an high percentage of error, however, has been possible to understand correlation between real C-arm movement and RDSR information.

Since the TLDs were distributed along phantom slices (from 12 to 19), the absorbed dose measured by TLDs are showed in the same order and paired with the skin dose from software. Since the phantom resolution is set to fine and the distance between points is less than 2 cm, points spaced closer than 1 cm from same TLD are averaged. Firstly, is observed a similar trend in slices for both types but value difference is already visible.

Statistical analysis is performed calculating mean values and standard error for every slice and for total. Is observed that only the values of TLDs and skin dose map (SDM) of slices 13 and 18 are statistically equal, but keeping in consideration the previous evaluation in Table 14.1, is possible to include the two dashed lines in Figure 14.7. These lines represent the TLDs mean measurement error of  $\pm 31.2\%$ . After this correction can be said that the software outputs result quite reliable, however is necessary other tests to confirm this hypothesis because of a huge TLD measurement error. Moreover, must remember the Air Kerma values of RDSRs can have a deviation of  $\pm 35\%$  per IEC and FDA that certainly affect the software results.

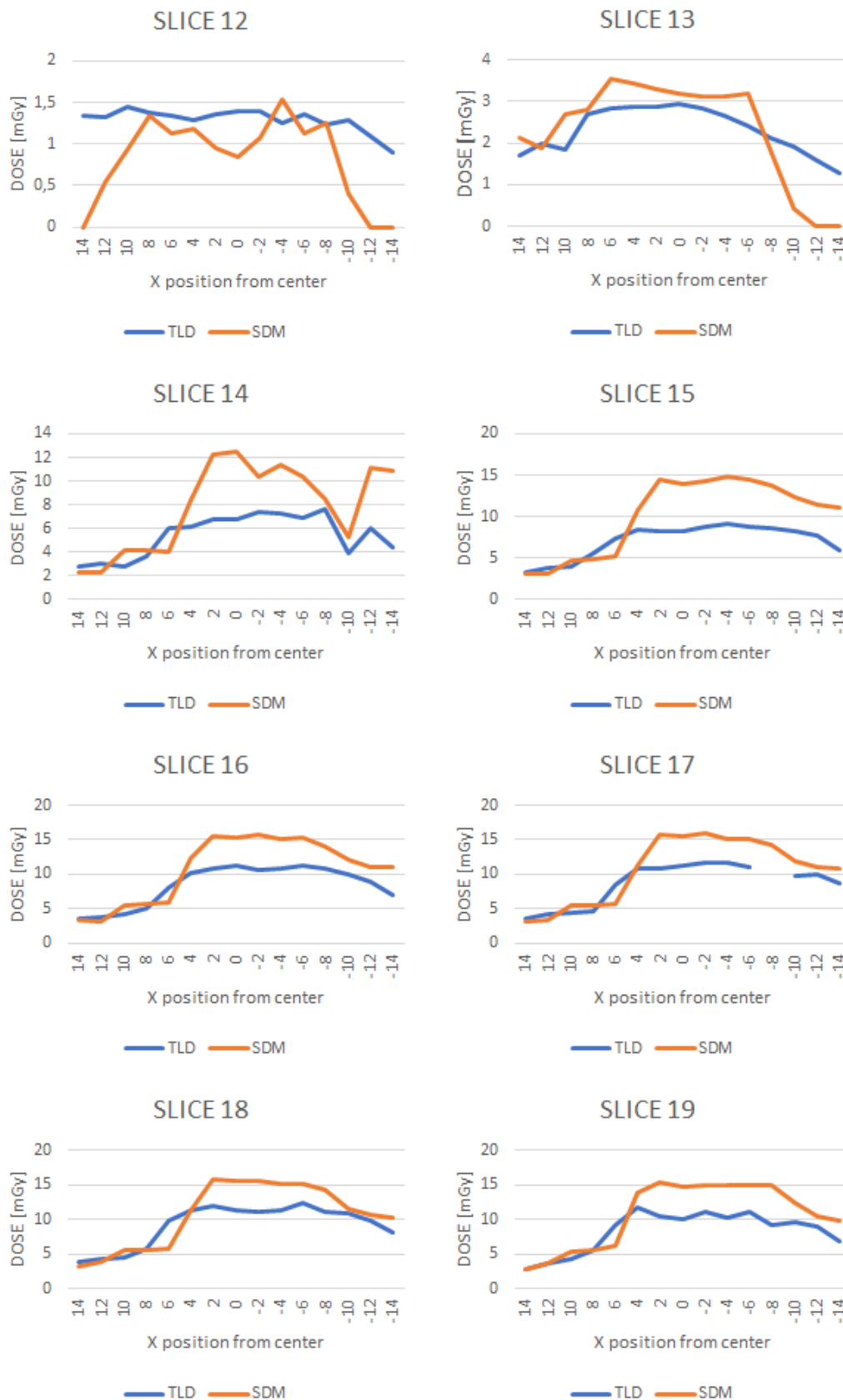


FIGURE 14.6: Dose distribution along x axis per slice.

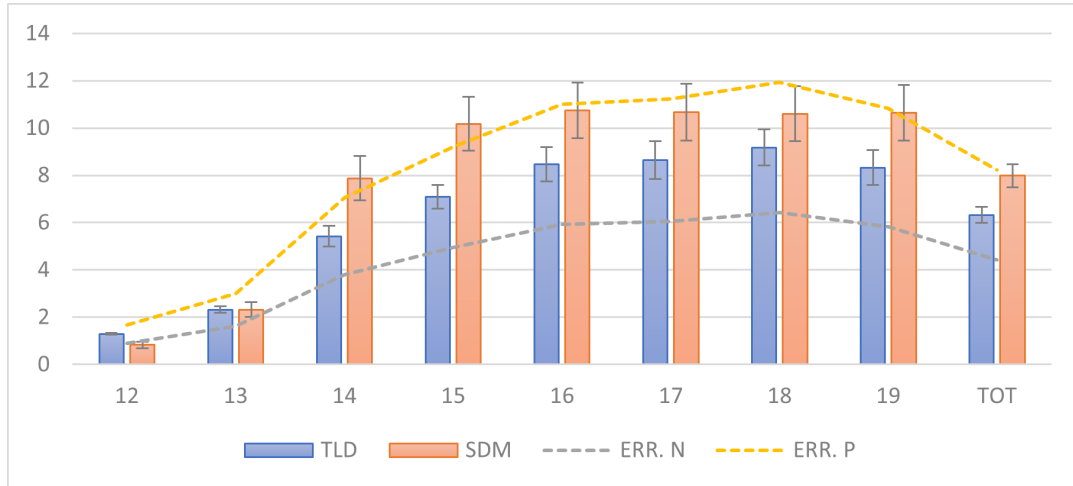


FIGURE 14.7: Mean values of absorbed dose per slice.

TABLE 14.2: Values of histograms

SLICE	TLD		SDM		TLD Measurement error	
	MEAN	STD.ERR.	MEAN	STD.ERR.	ERR. N	ERR. P
12	1,290	0,035	0,820	0,127	0,903	1,678
13	2,309	0,137	2,313	0,310	1,616	3,002
14	5,423	0,449	7,871	0,935	3,796	7,050
15	7,079	0,499	10,173	1,141	4,955	9,202
16	8,473	0,726	10,749	1,178	5,931	11,015
17	8,639	0,796	10,672	1,193	6,047	11,231
18	9,179	0,754	10,598	1,168	6,425	11,932
19	8,325	0,732	10,640	1,176	5,828	10,823
TOT	6,320	0,333	7,979	0,497	4,424	8,216

## Chapter 15

# Future work

The proposed methodology for calculating skin dose from fluoroscopic procedures includes all major physical corrections required. However, will be improve the calculation of correction factors trying to replicate used values. Since accuracy of ionization chamber of machine is  $\pm 35\%$ , will be recommended to introduce a new correction factor such that air kerma from RDSR is equal to real delivered value, hence reducing uncertainty. This parameter is named "calibration factor" and it was introduced by A. K. Wunderle (Wunderle, 2016). The phantom could be improved with the realization of a new phantom from CT or MRI exams of several patients in order to get better phantom-patient matching. Moreover, to improve the software accuracy will be necessary to perform new test with phantom and finally with real patient. Until present date, no such commercial systems have been readily available on the market, but study conducted by Omar et al (Omar et al., 2016), has reported the possible solution for monitoring the radiation dose absorbed by organs other than skin, in almost real-time during the XA intervention, utilizing the reference air kerma information from DICOM RDSR and geometry reconstruction, and in addition, performing the Monte Carlo simulations to obtain the absorbed dose within the tissue for inner organs. The PCXMC software tool, developed by STUK, can perform the inner organ dose estimation, based on MC simulations, but the needed parameters for calculation, need to be entered manually by operator, hence the process of organ dose estimation is not fully automated. A new project idea can be programming a standalone software that works online during examination, such that operator can manage absorbed dose before happens skin injuries. In addition, the software should automatically perform Monte Carlo simulation per event in order

to obtain real time correction factors for organ dose estimation.

## Appendix A

# Parameter description

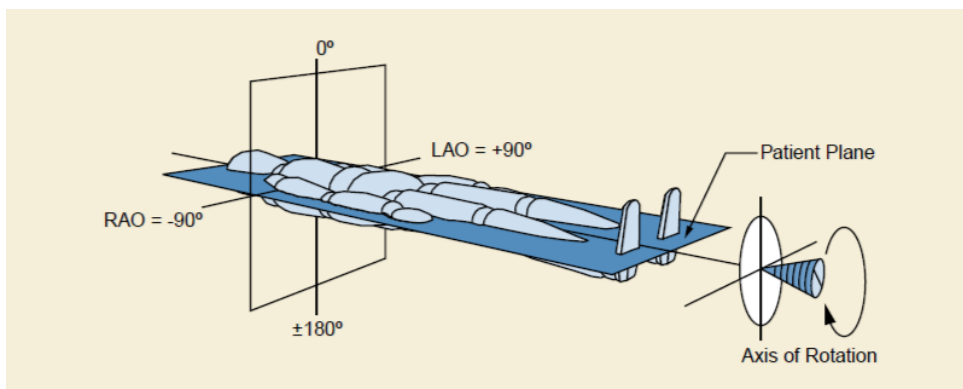


FIGURE A.1: Positioner Primary Angle.

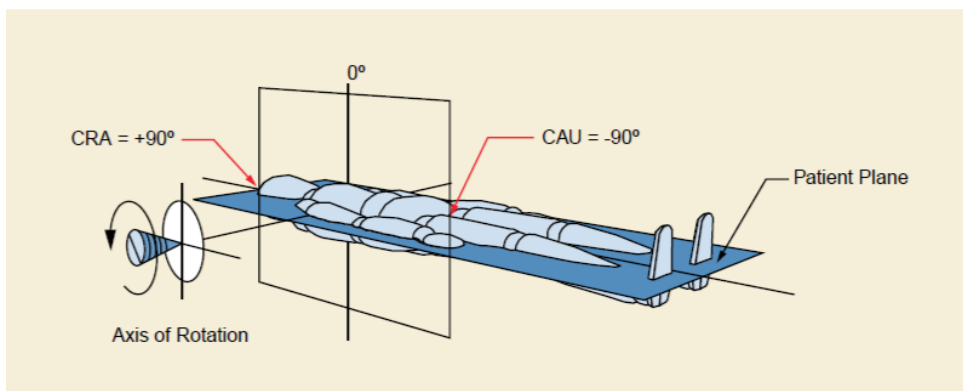


FIGURE A.2: Positioner Secondary Angle.

TABLE A.1: Description of RDSR parameters

CID	Parameter	Description	SI
113751	Table Longitudinal Position	Table Longitudinal Position with respect to an arbitrary chosen reference by the equipment. Table motion towards LAO is positive assuming that the patient is positioned supine and its head is in normal position.	mm
113753 /021	Table Height Position	Table Height Position with respect to an arbitrary chosen reference by the equipment. Table motion downwards is positive.	mm
113752	Table Lateral Position	Table Lateral Position with respect to an arbitrary chosen reference by the equipment. Table motion towards CRA is positive assuming that the patient is positioned supine and its head is in normal position.	mm
113748	Distance Source to Isocenter	Distance from the X-Ray Source to the Equipment C-Arm Isocenter.(Center of Rotation).	mm
112011	Positioner Primary Angle	Position of the X-Ray beam about the patient from the RAO to LAO direction where movement from RAO to vertical is positive.	degrees
112012	Positioner Secondary Angle	Position of the X-Ray beam about the patient from the caudal to cranial direction where movement from caudal to vertical is positive.	degrees
113736	Exposure	Mean value of X-Ray Current Time product.	mAs
113733	KVP	Applied X-Ray Tube voltage at peak of X-Ray generation; Mean value if measured over multiple peaks (pulses).	kV
113772	X-Ray Filter Type	Type of filter(s) inserted into the X-Ray beam.	
113757	X-Ray Filter Material	X-Ray absorbing material used in the filter.	
113758	X-Ray Filter Thickness Minimum	The minimum thickness of the X-Ray absorbing material used in the filters.	mm
113773	X-Ray Filter Thickness Maximum	The maximum thickness of the X-Ray absorbing material used in the filters.	mm
113764	Acquisition Plane	Identification of Acquisition Plane with Biplane systems.	
113721	Irradiation Event Type	Denotes the type of irradiation event recorded.	

<b>CID</b>	<b>Parameter</b>	<b>Description</b>	<b>SI</b>
113780	Reference Point Definition	System provided definition of the Reference Point used for Dose calculations.	
122130	Dose Area Product	Radiation dose times area of exposure.	Gym2
113738	Dose (RP)	Dose applied at the Reference Point (RP).	Gy
113734	X-Ray Tube Current	Mean value of applied Tube Current.	mA
113750	Distance Source to Detector	Measured or calculated distance from the X-Ray source to the detector plane in the center of the beam.	mm
123014	Target Region	Anatomic Region to be imaged.	
001	Height of System	Distance of Isocenter from floor.	mm
113745	Patient Table Relationship	Orientation of the Patient with respect to the Head of the Table.	
113743	Patient Orientation	Orientation of the Patient with respect to Gravity.	
113744	Patient Orientation Modifier	Enhances or modifies the Patient orientation specified in Patient Orientation.	
005	Wedges and Shutters	Collimator dimension.	
015	Longitudinal Beam Position	Distance of C-arm from a reference point defined by manufacturer.	
113793	Pulse Width	(Average) X-Ray pulse width.	ms
113768	Number of Pulses	Number of pulses applied by X-Ray systems during an irradiation event (acquisition run or pulsed fluoro).	



# Bibliography

- Benmakhlouf et al. (2011). "Backscatter factors and mass energy-absorption coefficient ratios for diagnostic radiology dosimetry". In: *Physics in Medicine and Biology* 56, 7179–7204.
- Cameron, John (1991). "Radiation Dosimetry". In: *Environmental Health Perspectives* 91, pp. 45–48.
- Hellström, M. (2018). "Estimating patient peak skin dose with fluoroscopic procedures".
- Herold, D. M., A. L. Hanlon, and G. E. Hanks (1999). "Diabetes mellitus: a predictor for late radiation morbidity". In: *Int J Radiat Oncol Biol Phys* 43, pp. 475–479.
- Hymes, S. R., E. A. Strom, and C. Fife (2006). "Radiation dermatitis: clinical presentation, pathophysiology, and treatment 2006". In: *Journal of the American Academy of Dermatology* 54.1, pp. 28–46.
- IAEA, International Atomic Energy Agency (2007). *Dosimetry in diagnostic radiology: an international code of practice*.
- ICRP (2007). "The 2007 recommendations of the International Commission on Radiological Protection. ICRP Publication 103". In: *Annals of the ICRP* 37.2-4, pp. 1–333.
- ICRU (2005). *ICRU Report 74. Patient dosimetry for x rays used in medical imaging*. Vol. 5.
- IEC (2010). "IEC 60601-2-43. 2nd edition". In.
- Koenig, T. R. et al. (2001). "Skin injuries from fluoroscopically guided procedures: part 1, characteristics of radiation injury". In: *AJR Am J Roentgenol* 177, pp. 3–11.
- Malchair, F. et al. (2020). "Review of skin dose calculation software in interventional cardiology". In: *Physica Medica* 80, pp. 75–83.
- Omar, A. et al. (2016). "A framework for organ dose estimation in x-ray angiography and interventional radiology based on dose-related data in DICOM structured reports". In: *Physics in Medicine and Biology* 61, pp. 3063–3083.

- Petoussi-Henss, N. et al. (1998). "Calculation of backscatter factors for diagnostic radiology using Monte Carlo methods". In: *Physics in Medicine and Biology* 43, 2237–2250.
- Pianykh, O. S. (2008). *Digital Imaging and Communications in Medicine*.
- Tapiovaara, M. and T. Siiskonen (2008). "PCXMC A Monte Carlo program for calculating patient doses in medical x-ray examinations (2nd Ed.)" In.
- Valentin, J. (2007). "Avoidance of radiation injuries from medical interventional procedures. ICRP Publication 85". In: *Annals of the ICRP* 30.2.
- Wunderle, Kevin Arthur (2016). "X-Ray Beam Characteristics And Radiation Dose Deposition To Soft Tissue From Fluoroscopic". In.